

# Dynamics of the cytokinetic ring in weak flow coupling limit

Mainak Chatterjee, Arkya Chatterjee<sup>1</sup>, Amitabha Nandi, and Anirban Sain<sup>2</sup>

*Department of Physics, Indian Institute of Technology-Bombay, Powai, Mumbai 400076, India*

(Dated: July 28, 2020)

Contraction of the cytokinetic ring during cell division leads to physical partitioning of a cell into two daughter cells. This contraction involves flows of actin filaments and myosin motors in the growing membrane interface that causes this separation. Within a continuum gel theory framework, we explore a weak flow coupling approximation where the dynamics of the order parameter, namely the degree of alignment of the acto-myosin filaments, is not significantly affected by the flow, however the flow is influenced by the active stresses generated by the filaments. This allows exact solution of the dynamical equations, producing good agreement with experimental observations. While the relevant time scale of the dynamics turns out to be the ratio of flow viscosity and acto-myosin activity, our theory captures how the effective tension in the ring decreases with its radius. We show how this effect significantly slows down the contraction process at later times.

PACS numbers: 87.16.Ka, 87.16.ad, 87.16.dj, 87.17.Ee

Cell division is fundamental to all living organisms. The last stage of cell division is cytokinesis, when a membrane interface grows radially inward at the equatorial plane of the cell (see Fig.1a) and separates it into two daughter cells [1]. Such interfaces are common in dividing cells in tissues. Here we focus on mitotic cell division in *C. elegans* embryo, a widely studied model system for eukaryotes. The growth of the interface is driven by the constriction of a contractile ring which forms at the inner edge of the annular shaped interface (see Fig.1b). The ring is made of actin filaments and myosin motors [1, 2]. It forms due to the flow of actin and myosin, beneath the cell surface (*the cortical flow*), from the polar to the equatorial region of the dividing cell [3]. Experiments suggest [1, 2, 4] that the ATP driven interaction between actin and myosin lead to the generation of *active* contractile stresses in the cytokinetic ring. How this stress changes with time during the course of the constriction however is not clear. Earlier theoretical models [5, 6] explain the observed contraction rate by assuming a constant contractile stress. Ref[7] had in addition assumed, on phenomenological grounds, a dynamic component to the stress that causes an eventual slowdown of the contraction process.

Such an approach, that considers the actin ring to be a separate entity attached with the growing active membrane, cannot explain the recent experimental observations [8] where the ring is found to reorganize and constrict even after part of it is destroyed by localized laser ablation. This motivates us to consider the cortical ring to be part of the acto-myosin continuum spread over the growing membrane. In Ref[9], the authors discussed an active gel model of the cytoskeletal flows leading to actin ring formation and contraction, in the context of wound healing in *Xenopus* oocyte [10]. Such a description involves solution of coupled equations for the actin alignment field  $Q_{\alpha\beta}(r)$  (the order parameter) and the velocity field  $v_\alpha(r)$ . The ring was assumed to be a narrow annular

zone with higher level of myosin activity  $\zeta\Delta\mu$  and higher degree of actin alignment than the rest of the growing cortex.

In this Letter, we follow a similar continuum gel theory approach but simplify the dynamical equations first by ignoring the flow coupling of the order parameter field. This is a reasonable approximation when the velocity field is slow compared to the internal dynamics of the order parameter field. Such an approximation has been recently explored in the context of tissue spreading also [11, 12]. Crucial to our theory is a phenomenological input that the actin filaments get highly aligned in the ring, tangential to the open boundary. These allow rotationally symmetric analytical solutions for the  $Q_{\alpha\beta}(r)$  and the  $v_\alpha(r)$  fields. As we will see later, these solutions agree well with experimental observations and provide insight into certain aspects of the dynamics that was not understood before.

The actomyosin gel on the growing interface is modeled as a nematic fluid. Orientational order in a nematic fluid, in 3-dimensions, is defined by the tensor order parameter  $Q_{\alpha\beta} = \langle n_\alpha n_\beta - \delta_{\alpha\beta}/3 \rangle$ , where  $n_\alpha$  is the nematic director field, and  $\alpha, \beta = (x, y, z)$ . As the acto-myosin filaments (nematic directors) lie in the flat interface ( $x - y$ ), symmetry and tracelessness of  $Q_{\alpha\beta}$  dictate, that the non-diagonal matrix elements involving  $z$  are zero,  $Q_{xy} = Q_{yx} = q$ ,  $Q_{zz} = -1/3$ , and  $Q_{xx} + Q_{yy} = 1/3$ . Further, if the orientation distribution is isotropic in the  $x - y$  plane then the resulting matrix  $Q_{\alpha\beta}^0$  is diagonal, with  $Q_{xx}^0 = Q_{yy}^0 = 1/6$ , and  $Q_{zz}^0 = -1/3$ . In the presence of cortical flows or due to specific boundary conditions the isotropic distribution is modified to  $Q_{\alpha\beta} = Q_{\alpha\beta}^0 + Q'_{\alpha\beta}$ . Again symmetric structure and tracelessness of  $Q_{\alpha\beta}$  require (see Supplementary information -SI) that,  $Q'_{xx} = -Q'_{yy} = \tilde{Q}$ ,  $Q'_{xy} = Q'_{yx} = q$ , and rest of the elements are zero. This form remains invariant as we transform from cartesian to 2D polar coordinates later.

*Active gel model for acto-myosin filaments* : The free

energy of the inhomogeneous nematic field can be described by the Landau-De Gennes form [13], using the  $Q'$  matrix.

$$\mathcal{F} = \int d^3r \left( \frac{\chi}{2} Q'_{ij} Q'_{ji} + \frac{L}{2} \partial_k Q'_{ij} \partial_k Q'_{ij} \right). \quad (1)$$

This enforces an isotropic nematic arrangement in the bulk of the 2D growing cortical layer with a correlation length  $L_c = \sqrt{L/\chi}$ . Later, we will see that this turns out to be the width of the actomyosin ring, which has been measured [14] to be  $\sim 1\mu m$ .

Constitutive equations of the active gel can be described by a linear relationship between thermodynamic fluxes and forces (see, for example, [9, 15–17]). We choose stress tensor  $\sigma_{\alpha\beta}$ , the rate of change of nematic order parameter  $\frac{DQ_{\alpha\beta}}{Dt}$ , and the rate of ATP consumption as the fluxes. The conjugate forces are the strain rate  $v_{\alpha\beta} = \frac{1}{2}(\partial_\alpha v_\beta + \partial_\beta v_\alpha)$ , the traceless nematic force field  $H_{\alpha\beta} = -\frac{\delta\mathcal{F}}{\delta Q_{\alpha\beta}}$ , and the chemical potential difference generated due to ATP hydrolysis  $\Delta\mu$ . Following [9] the hydrodynamic equations in the liquid limit can be expressed as follows:

$$\sigma_{\alpha\beta} = 2\eta v_{\alpha\beta} - \beta_1 H_{\alpha\beta} + \zeta \Delta\mu Q_{\alpha\beta}, \quad (2)$$

$$\frac{D}{Dt} Q_{\alpha\beta} = \beta_1 v_{\alpha\beta} + \frac{1}{\beta_2} H_{\alpha\beta}. \quad (3)$$

$\frac{D}{Dt}$  here implies material derivative [15],  $\zeta \Delta\mu Q_{\alpha\beta}$  is the active stress and contractility of the cortical layer enforces  $\zeta > 0$  [15, 16]. For simplicity we ignored any explicit active term in the second equation. Here  $\eta$  is the fluid viscosity while  $\beta_1$  and  $\beta_2$  are Onsager coefficients [9], and give the flow coupling and nematic relaxation strengths, respectively [9].

Following [9], we define a 2D “tension tensor”  $t_{ij}$  via the relation  $t_{ij} = \int (\sigma_{ij} - \delta_{ij} P) dz$ . Imposing the net normal stress on the interface  $t_{zz}$  to be zero yields pressure  $P = \sigma_{zz}$ . Further, ignoring variation of stress across the thin interface, we get [9]  $t_{ij} = e(\sigma_{ij} - \delta_{ij} \sigma_{zz})$ , where  $e$  is the effective thickness of the interface, assumed to be a constant here. This tension tensor allows us to write a two-dimensional hydrodynamic theory as follows

$$\frac{\partial}{\partial t} (\rho v_i) = \partial_j t_{ij} - \alpha v_i \quad (4)$$

where  $\alpha$  is the cytoplasmic friction external to the growing membrane interface. In the highly viscous regime, we drop the time derivative to get  $\partial_j t_{ij} = \alpha v_i$ . In the following analysis we make a simplifying assumption mentioned before [11, 12]; we ignore flow coupling i.e.,  $\beta_1 \simeq 0$ . Under these assumptions, Eq(3) yields  $H_{\alpha\beta} = 0$ . Evaluating  $H_{\alpha\beta}$ , using Eq.1, we obtain

$$\nabla^2 \tilde{Q} = \frac{\tilde{Q}}{L_c^2}, \text{ and } \nabla^2 q = \frac{q}{L_c^2}. \quad (5)$$

We assume the flat growing interface to have an annular shape, see of Fig.1b. The shrinking cytokinetic ring of radius  $R_0(t)$  lies at its inner periphery, while its outer periphery is fixed at radius  $r_0$ . We transform our equations to 2D polar coordinates in order to take advantage of the circular symmetry in the  $x - y$  plane. The  $2 \times 2$  ( $xy$ ) block of  $Q'_{\alpha\beta}$  matrix (anisotropic part) remains traceless and symmetric, parameterised by two variables  $\tilde{Q}$  and  $q$ , although their values depend on the particular coordinate frame used (polar here). The  $2 \times 2$  block of the isotropic matrix however remains unchanged,  $Q_{\alpha\beta}^0 = \mathbb{I}/6$ , where  $\mathbb{I}$  is the  $2 \times 2$  identity matrix (see SI for details).

The strain rates  $v_{\alpha\beta}$  in 2D polar coordinates read

$$v_{\alpha\beta} = \begin{bmatrix} \partial_r v_r & \frac{1}{2} \left\{ \frac{1}{r} \partial_\theta v_r + r \partial_r \left( \frac{v_\theta}{r} \right) \right\} \\ \frac{1}{2} \left\{ \frac{1}{r} \partial_\theta v_r + r \partial_r \left( \frac{v_\theta}{r} \right) \right\} & \frac{1}{r} (v_r + \partial_\theta v_\theta) \end{bmatrix} \quad (6)$$

and the force balance equations, Eq.(4) are

$$\partial_r t_{rr} + \frac{1}{r} (t_{rr} - t_{\theta\theta}) + \frac{1}{r} \partial_\theta t_{r\theta} = \alpha v_r \quad (7a)$$

$$\partial_\theta t_{\theta r} + \frac{1}{r} (t_{\theta r} + t_{r\theta}) + \frac{1}{r} \partial_\theta t_{\theta\theta} = \alpha v_\theta \quad (7b)$$

*Rotationally symmetric solutions for  $Q'_{\alpha\beta}(r)$  and  $v_\alpha(r)$ :* We first consider the special case where the circular ring is at  $r = R_0$ , with our domain of interest  $r \geq R_0$ . We start with  $\alpha = 0$ , set stress free boundary condition at the open edge, i.e., normal stress  $\sigma_{rr}(R_0) = 0$ , and  $v_r = 0$  at  $r \rightarrow \infty$ . The nematic directors are assumed to be parallel to the inner boundary, i.e.,  $\hat{n}(R_0) = \hat{\theta}$ , and isotropic as  $r \rightarrow \infty$ . It implies, that at  $r = R_0$ , the anisotropic  $Q'_{\alpha\beta}$  matrix is diagonal with  $Q'_{rr} = -Q'_{\theta\theta} = \tilde{Q} = -1/2$  (see SI), and  $Q'_{\alpha\beta}(r = \infty) = 0$ . We rewrite Eq.5, for  $Q$  and  $q$ , in their polar form (see SI) :

$$\frac{\partial}{\partial r} \left( r \frac{\partial \tilde{Q}}{\partial r} \right) - \left( \frac{r}{L_c^2} + \frac{4}{r} \right) \tilde{Q} = 0, \text{ and identically for } q. \quad (8)$$

The general solution is  $\tilde{Q}^0(r) = c_1 K_2(r/L_c) + c_2 I_2(r/L_c)$ , where  $K_2$  and  $I_2$  are modified Bessel functions. Boundary conditions yield

$$\tilde{Q}^0(r) = -\frac{K_2(r/L_c)}{2K_2(R_0/L_c)}. \quad (9)$$

Combining Eq.7b and the equation for  $q(r)$  in Eq.8, we get  $q(r) = 0$  (see SI). The zeroth order solution  $\tilde{Q}^0$  in Eq.9 is shown in the inset of Fig.1. The sharp rise in the magnitude of  $\tilde{Q}$  at the inner edge can be interpreted as the acto-myosin ring, of width  $L_c$ . Using this solution we can now solve Eq.7b for  $v_r$ ,

$$4\eta \frac{\partial}{\partial r} \left( \frac{\partial}{\partial r} + \frac{1}{r} \right) v_r = -\zeta \Delta\mu \left( \frac{\partial}{\partial r} + \frac{2}{r} \right) \tilde{Q}, \quad (10)$$

with the boundary conditions,

$$v_r(\infty) = 0, \text{ and } \sigma_{rr}(R_0) = 2\eta \partial_r v_r + \frac{\zeta \Delta\mu}{6} + \zeta \Delta\mu \tilde{Q} = 0. \quad (11)$$

The resulting inward moving velocity field is given below and is plotted in Fig.1, using  $L_c$  as unit of length and  $\frac{\eta}{\zeta\Delta\mu}$  as unit of time.

$$v_r^0(r) = -\frac{\zeta\Delta\mu}{\eta} \left[ \left( 1 + \frac{3K_1'(R_0/L_c)}{4K_2(R_0/L_c)} \right) \frac{R_0^2}{6r} + \frac{L_c}{8} \frac{K_1(r/L_c)}{K_2(R_0/L_c)} \right]$$

The velocity at  $r = R_0$ , is the ring closure rate.

$$v_r^0(R_0) = -\frac{\zeta\Delta\mu}{\eta} \frac{R_0}{6} \left[ 1 - \frac{3K_0(R_0/L_c)}{4K_2(R_0/L_c)} \right] \quad (13)$$

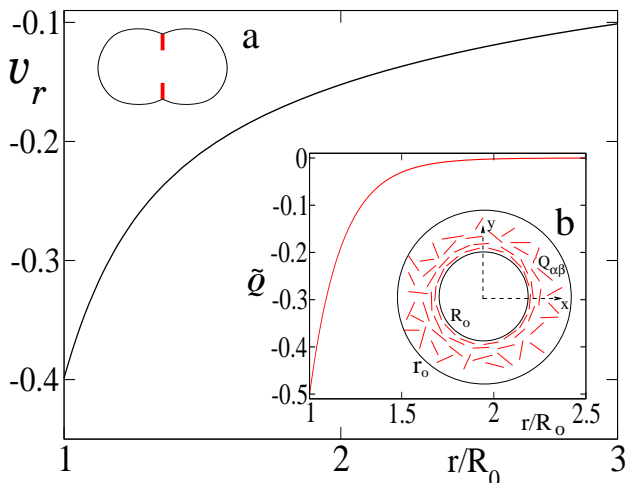


Figure 1: The zeroth order solution for the radially symmetric velocity field  $v_r^0(r)$ , shown as a function of  $r/R_0$ , for  $R_0 = 5\mu\text{m}$ . The inset shows  $\tilde{Q}^0(r)$  as a function of  $r/R_0$ . Schematic diagram 'a' shows sideview of the growing interface at the middle of the cell and 'b' shows its cross-sectional view. Alignment of filaments increases sharply near the inner boundary of the annulus at  $R_0$ . The outer boundary is fixed at  $r_0 = \infty$  for these plots.

While these zeroth order solutions reveal the inhomogenous nature of the cortical flow and the filament orientation field, comparison to experiments requires inclusion of other realistic features.

*Effect of finite outer radius  $r_0$  and cytoplasmic friction* : Realistic boundary conditions that both  $\tilde{Q}$  and  $v_r$  go to zero at finite outer radius  $r_0 > R_0$  (instead of  $r_0 = \infty$ ), makes the solutions little more complex. The new exact solution for  $\tilde{Q}(r)$ , where both  $K_2$  and  $I_2$  contribute, is given in SI. The corresponding solution for the velocity  $v_r$  is obtained numerically using Mathematica. Further, inclusion of cytoplasmic friction in the force balance equation adds  $\alpha v_r$  to the right hand side of Eq.10. Restricting ourselves to radial motion only ( $v_r$  nonzero,  $v_\theta = 0$ ) and azimuthal symmetry, we get

$$\left[ \partial_r \left( \partial_r + \frac{1}{r} \right) - \frac{\alpha}{4\eta} \right] v_r = -\frac{\zeta\Delta\mu}{4\eta} \left( \partial_r + \frac{2}{r} \right) \tilde{Q}. \quad (14)$$

We can use  $\tilde{Q} = \tilde{Q}^0$ , since the friction does not change Eq.10, while we still ignore flow coupling (i.e.,  $\beta_1 = 0$ ). With boundary conditions  $\tilde{Q} = v_r = 0$  at  $r = r_0$ , and those at  $r = R_0$  remaining same as before, we solve Eq.14, both using Green's function (see SI) and numerically in Mathematica. As expected, see Fig.2, cytoplasmic friction damps the cortical velocity, and slows down the ring closure speed (inset of Fig.2).

The above analysis is carried out quasi-statically for a fixed  $R_0$ . We can use these results to obtain the ring closure kinetics. We integrate the kinematic boundary condition  $\frac{d}{dt}R_0 = v_r(R_0)$  to derive the time dependence of the radius of the contracting ring i.e.,  $R_0$  versus  $t$ . In Fig.2-inset we compare this closure rate with experimental data on *C. elegans* embryo [5, 18]. We use  $L_c$  ( $1\mu\text{m}$ ) [18]) as unit of length and  $\frac{\eta}{\zeta\Delta\mu}$  as unit of time. The theoretical result fits the experimental data well and from the fit we obtain  $\frac{\eta}{\zeta\Delta\mu} \simeq 2.15$  sec and the friction constant  $\alpha \simeq 0.7$ . Membrane tension  $\sigma_0$  in the growing membrane can be linked to the activity as  $\sigma_0 = \zeta\Delta\mu e/2$  [9]. Using measured value of cortical tension  $\sigma_0 = 3 \times 10^{-4} \text{N/m}$  [19] and the thickness of the growing actomyosin cortex  $e \sim 0.3\mu\text{m}$  [18], we get  $\eta \sim 4 \times 10^3 \text{Pa}\cdot\text{sec}$ , which is

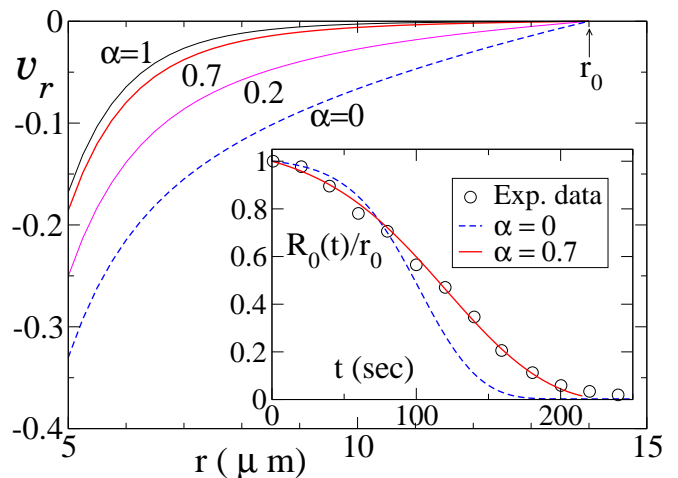


Figure 2: Cytoplasmic friction slows down the cortical flow:  $v_r$  versus  $r$  is shown in the main plot for different values of the friction coefficient  $\alpha$ . Scaled radius of the ring,  $R_0(t)/r_0$  versus time is shown in the inset. The outer radius is fixed at  $r_0 = 14\mu\text{m}$ . The inset shows that theoretical result (solid line) match well with experimental data on *C. elegans* embryo (circles) [5, 18] when cytoplasmic friction and realistic finite outer boundary are incorporated in the theory.

The ring closure rate in eukaryotes shows an intriguing slow down at late times, which has not been understood yet. Reduction in the effective ring tension or increase in internal friction have been proposed as possible reasons. In Ref[7] an intrinsic dynamic friction  $\zeta_L$  was added, on phenomenological grounds, to the ring tension to account for hitherto unknown internal processes in the ring. In

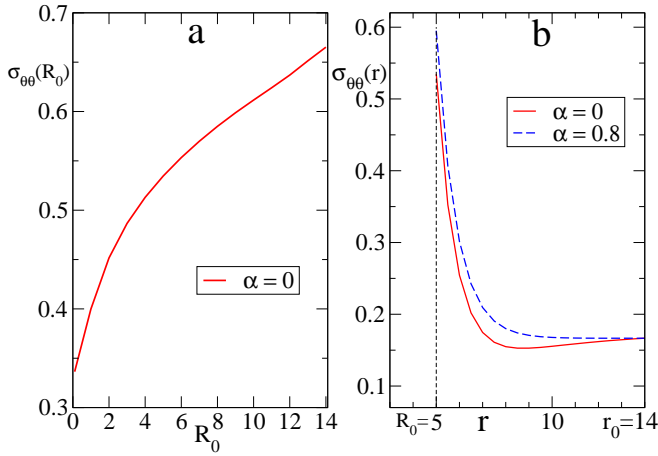


Figure 3: The line tension, (Eq.15), at the ring  $\Sigma = \sigma_{\theta\theta}(R_0)$ , in units of activity  $\zeta\Delta\mu$ , shown as a function of ring radius  $R_0$  (in a), and as a function of  $r$  (in b), at a fixed  $R_0 = 5\mu m$ . The outer radius is fixed at  $r_0 = 14\mu m$ , appropriate for *C. elegans* embryo [5, 18]. Friction (nonzero  $\alpha$ ) does not affect ring tension significantly.

our present theory  $\sigma_{\theta\theta}(r = R_0)$  is equivalent to the ring tension  $\Sigma$  of Ref[7]. From Eq.2,

$$\sigma_{\theta\theta} = 2\eta\frac{v_r}{r} + \frac{\zeta\Delta\mu}{6} - \zeta\Delta\mu\tilde{Q}. \quad (15)$$

In Fig.3a we show the ring tension as a function of the ring size  $R_0$ , and Fig.3b shows how azimuthal stress varies in the bulk of the closing interface, for a given ring size  $R_0$ . First,  $\sigma_{\theta\theta}$  is always positive, implying contractile stress in the ring and the interface. Second, the ring tension falls sharply at small  $R_0$ , which explains the slow down. Third, the azimuthal stress  $\sigma_{\theta\theta}(r)$  is very high at the edge  $r = R_0$  and small in the interior. This property perfectly justifies the role of the ring as the main generator of cytokinetic tension. Note, that in Eq.15 the last two terms on the right hand side are constants (at the ring  $r = R_0$ ), and positive. But the first term is negative and its magnitude grows large as the hole shrinks, eventually reducing the line tension. So the slowing down effect appears naturally due to viscosity of the flowing gel and curvature of the ring. Interestingly this tension reduction term has the same structure  $v_r(R_0)/R_0 = \dot{R}_0/R_0$  which was assumed in Ref[7], based on phenomenology.

*Effect of flow coupling :* We now examine, the effect of weak flow coupling ( $\beta_1 \leq 1$ ) on Eq.2 and 3. To separate the effects of flow coupling and cytoplasmic friction, here we set  $\alpha = 0$ , but retain a finite outer periphery at  $r_0 = 14\mu m$ . At steady state, Eq.3 implies  $H_{\alpha\beta} = \beta_1\beta_2v_{\alpha\beta}$ , which gives Eq.16 below. However the  $q = 0$  solution remains unchanged. Substitution of  $H_{\alpha\beta}$  into Eq.2 simply renormalizes the viscosity  $\eta \rightarrow \eta + \frac{1}{2}\beta_1^2\beta_2$ . The resulting velocity equation (Eq.17 below) has the same form as Eq.10.

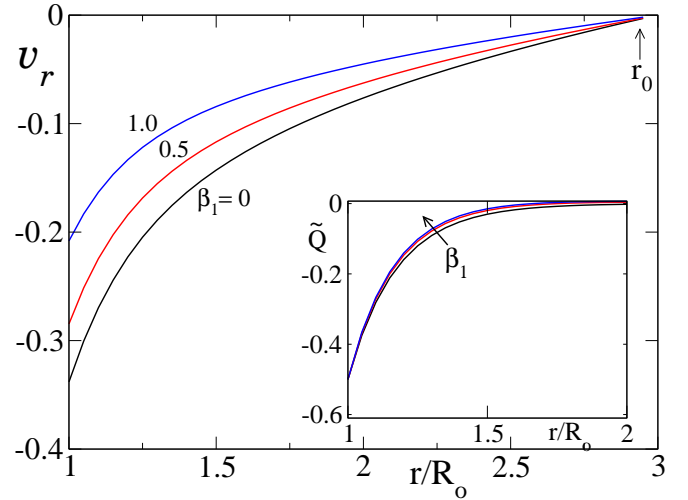


Figure 4: Velocity field shown as a function of  $r$ , at different values of flow coupling strength,  $\beta_1 = 0, 0.5$  and  $1$ , keeping  $R_0 = 5\mu m$  fixed. The corresponding order parameter plots ( $\beta_1$  increasing in the direction of the arrow) are shown in the inset.

$$\partial_r (r\partial_r)\tilde{Q} - \left(\frac{r}{L_c^2} + \frac{4}{r}\right)\tilde{Q} = -\frac{\beta_1\beta_2}{2L}r(\partial_r v_r - \frac{v_r}{r}) \quad (16)$$

$$4\eta\partial_r\left(\partial_r + \frac{1}{r}\right)v_r = \frac{-\zeta\Delta\mu}{1+\beta_1^2\beta_2/2\eta}\left(\partial_r + \frac{2}{r}\right)\tilde{Q} \quad (17)$$

We solve these two coupled equations numerically (using Mathematica), with the same boundary conditions as before (with  $L = 1, \eta = 1, \beta_2 = 1$ ), and the solutions are shown in Fig.4. It shows damping of the velocity field  $v_r$  with increase in flow coupling strength  $\beta_1$ . Therefore, flow coupling can potentially increase the ring closure time, however the order parameter is nearly unaffected by flow coupling.

In summary, our treatment of the ring as a part of the acto-myosin continuum, albeit in the weak flow coupling limit, produce analytical results that are consistent with experimental observations. We resolve how the effective ring tension decreases with time as constriction proceeds. While the actomyosin viscosity and curvature of the shrinking ring determine the slow down, both cytoplasmic friction and flow coupling can stretch this slow down further. This effect could be relevant for wound healing in tissues as well. For example, wound healing in *Drosophila* wing imaginal discs shows [21] a similar slow down which is attributed [21] to weakening of the actin purse-string, an inter-cellular structure similar to intra-cellular actin ring.

Acknowledgement: MC would like to thank IIT Bombay, India for financial support. AN and AS acknowledge Science and Engineering Research Board (SERB), India Project No. ECR/2016/001967 and CRG/2019/005944, respectively, for financial support.

<sup>1</sup> Present address: Physics Department, MIT, Cambridge

MA 02139, USA.

<sup>2</sup> asain@phy.iitb.ac.in

- 
- [1] R. Rappaport, *Cytokinesis in animal cells* (Cambridge University Press, 1996).
- [2] R. A. Green, E. Paluch, and K. Oegema, Annual review of cell and developmental biology **28**, 29 (2012).
- [3] D. Bray and J. White, Science **239**, 883 (1988).
- [4] J.-H. Zang and J. A. Spudich, Proceedings of the National Academy of Sciences **95**, 13652 (1998).
- [5] A. Zumdick, K. Kruse, H. Bringmann, A. A. Hyman, and F. Jülicher, PloS one **2** (2007).
- [6] H. Turlier, B. Audoly, J. Prost, and J.-F. Joanny, Biophysical journal **106**, 114 (2014).
- [7] A. Sain, M. M. Inamdar, and F. Jülicher, Physical review letters **114**, 048102 (2015).
- [8] A. M. Silva, D. S. Osório, A. J. Pereira, H. Maiato, I. M. Pinto, B. Rubinstein, R. Gassmann, I. A. Telley, and A. X. Carvalho, J Cell Biol **215**, 789 (2016).
- [9] G. Salbreux, J. Prost, and J.-F. Joanny, Physical review letters **103**, 058102 (2009).
- [10] C. A. Mandato and W. M. Bement, The Journal of cell biology **154**, 785 (2001).
- [11] R. Alert, C. Blanch-Mercader, and J. Casademunt, Physical review letters **122**, 088104 (2019).
- [12] C. Pérez-González, R. Alert, C. Blanch-Mercader, M. Gómez-González, T. Kolodziej, E. Bazellieres, J. Casademunt, and X. Trepát, Nature Physics **15**, 79 (2019).
- [13] P.-G. De Gennes and J. Prost, *The physics of liquid crystals*, vol. 83 (Oxford university press, 1993).
- [14] A. Carvalho, A. Desai, and K. Oegema, Cell **137**, 926 (2009).
- [15] K. Kruse, J.-F. Joanny, F. Jülicher, J. Prost, and K. Sekimoto, The European Physical Journal E **16**, 5 (2005).
- [16] M. C. Marchetti, J.-F. Joanny, S. Ramaswamy, T. B. Liverpool, J. Prost, M. Rao, and R. A. Simha, Reviews of Modern Physics **85**, 1143 (2013).
- [17] J. Prost, F. Jülicher, and J.-F. Joanny, Nature physics **11**, 111 (2015).
- [18] A. S. Maddox, L. Lewellyn, A. Desai, and K. Oegema, Developmental cell **12**, 827 (2007).
- [19] O. Thoumine, O. Cardoso, and J.-J. Meister, European Biophysics Journal **28**, 222 (1999).
- [20] F. Wottawah, S. Schinkinger, B. Lincoln, R. Ananthkrishnan, M. Romeyke, J. Guck, and J. Käs, Physical review letters **94**, 098103 (2005).
- [21] R. J. Tetley, M. F. Staddon, D. Heller, A. Hoppe, S. Banerjee, and Y. Mao, Nature physics **15**, 1195 (2019).